Dynamics of plume propagation and splitting during pulsed-laser ablation of Si in He and Ar

R. F. Wood, J. N. Leboeuf, D. B. Geohegan, A. A. Puretzky, and K. R. Chen*
Oak Ridge National Laboratory, P.O. Box 2008, MS 6032, Oak Ridge, Tennessee 37831-6032
(Received 7 November 1997)

A modeling approach for calculating the expansion of a laser-generated plasma into a background gas has been developed. Although relatively simple in structure, the model gives excellent fits to various experimental data for Si in background gases of He and Ar, including the previously unexplained ''splitting'' of the ablated plume. The model is based on a combination of multiple-scattering and hydrodynamic approaches. It allows the plume to be broken up into components, or scattering orders, whose particles undergo 0, 1, 2, . . . collisions with the background. Particles can only be transferred from one order to the next higher order by collisions. The densities in the individual orders propagate according to the usual conservation equations to give the overall plume expansion. When Ar is the background gas, there is a non-negligible probability that Si plume atoms will reach the detector without undergoing any collisions. This gives rise to a flux component that is undisplaced from that obtained when no background gas is present in addition to the delayed peak from the scattered flux. In Ar only a few orders are necessary for convergence. The behavior in the light gas He is more complex because of the relatively small effect of any one-scattering event and the calculations must be carried out in some cases to as high as the 12th scattering order to find agreement with the experiments. [S0163-1829(98)03827-2]

I. INTRODUCTION

During the past decade laser ablation has emerged as one of the most versatile techniques for the deposition of thin films of a variety of materials.[1,2] It has proved particularly useful in the deposition of thin films and superlattices of high-temperature superconductors.[3,4] The foundations of laser ablation lie in the much older field of laser-matter interactions where, from its very beginning, many materials were irradiated with high-power laser pulses.[5–7] Therefore, a study of the process has intrinsic relevance beyond the materials applications that will be emphasized here.

For the pulsed-laser deposition of materials,[8] the quality of the films depends critically on the range and profile of the kinetic energy and density of the laser-ablated plume. Consequently, the observed differences in plume dynamics when the ablation occurs with and without background gases is of crucial importance. In particular, the experimentally observed[7,9] splitting of the plume into an energetic component traveling at near vacuum speed and a component slowed by the ambient gas has been difficult to understand and to account for theoretically. This is a widely observed phenomenon occurring during ablation of single elements such as Si and Cu, as well as of complex compounds such as $YBa_2Cu_3O_7$ and in the presence of a variety of background gases such as Ar, N_2, and He.[9,10] In all instances, the background gas appears to act as a regulator of ablated plume energetics. It is important to know the constitution and dynamical behavior of the plume of material that is ablated from the target and deposited on the substrate, and to understand how the film-growth process can be controlled and optimized by varying the laser parameters, the target-substrate distance, and the introduction of various ambient gases into the deposition chamber. For example, it has been found that the fast component of the plume may cause damage to the growing film[11] and that this can be controlled to a certain extent by the pressure of the ambient gas. Also, clustering of film constituents in the gas phase or on the surface may cause problems or may provide a method of producing granular material or nanoparticles that may themselves be of technological importance.[8,12,13]

In this paper, we expand on our recent abbreviated reports on the simulation of plume dynamics[14,15] and give a detailed theoretical description of the phenomenon of plume splitting in background gases under conditions of interest for film growth. This has been made possible through the development of a modeling approach that describes quantitatively the behavior of a Si plume in the presence of He and Ar background gases. The dynamics of the background gas during the ablation process have also been extracted from the calculations. We will frequently refer to our approach as multiple scattering but, in fact, it can also be viewed as a combination of scattering and gas dynamical or hydrodynamical formulations. Although by necessity many approximations must be made to arrive at a tractable approach, the agreement between theory and experiment shows that the essential physics underlying the various phenomena has been retained.

After briefly reviewing the relevant experimental results and previous modeling efforts in the next section, we describe our approach in Sec. III and show in Sec. IV how the results coming from it provide a coherent understanding of experimental results whose interpretations were previously quite unclear. The paper concludes in Sec. V with a brief summary and a few concluding remarks about applications to other systems.

II. EXPERIMENTAL AND THEORETICAL BACKGROUND

A. Experiment

Careful consideration was given to the choice of an experimental system. Silicon was chosen for the target because

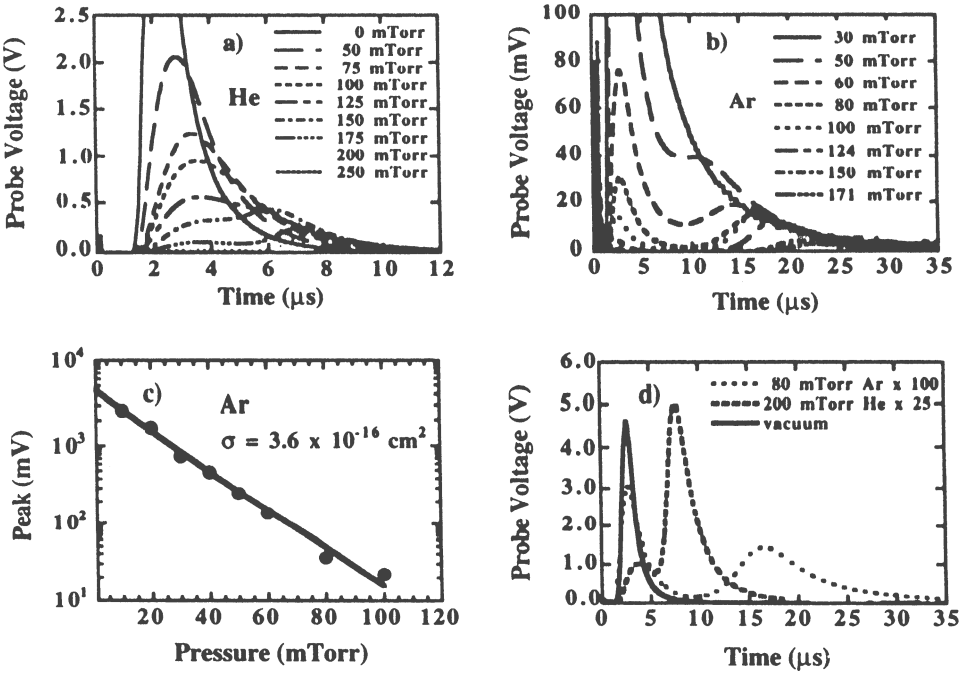

FIG. 1. Experimental results for ion probe measurements. Panels (a) and (b) show the fluxes at the detector located 5 cm from the target for He and Ar background gas, respectively, at the pressures indicated. Panel (c) shows the fall-off in intensity of the fast component of the flux as a function of Ar pressure. Panel (d) compares the results for Ar and He at the pressures indicated to illustrate the greatly different effects of the two gases.

it is well characterized, is readily obtained in pure single crystal form, is easy to work with, and has already been thoroughly studied in the laser-annealing regime of pulse-energy densities.[16] Rare gases, specifically He and Ar, were chosen because their first ionization energies are high (25 and 16 eV, respectively) and hence background ionization is more easily avoided. The energy density of the KrF laser pulses (duration time ~ 28 ns full width at half maximum) was chosen to be 3.0 J/cm^2 in order to obtain a good supply of singly ionized Si atoms for the ion-probe detector, while avoiding higher ionization states. Subsequent time-resolved emission and absorption spectroscopic measurements verified that only neutral and singly ionized Si were present in the plume and only neutral Ar and He in the background gas. A detailed description of the experimental setup and operation can be found in a recent paper by Geohegan.[17] We note here that a significant contribution of the recent experimental work has been the development of an array of diagnostic techniques with which to study plasma formation, plume propagation, light emission, etc. that occur during the laser-ablation process.[18]

The experimental results for background gases of He and Ar are given in Fig. 1. Panels (a) and (b) show plume-flux profiles measured by the ion-probe detector at 5 cm along the normal from the target as a function of time for several different pressures of the background gases, as noted.

Let us consider the results for Ar first because the plume splitting is more obvious in this case and because it also provides some direct insight into at least one feature of the splitting. It should be noted that although the sharp, main peak at ~ 2 μs decreases in intensity with the Ar pressure, its position is virtually independent of pressure. In fact, a good fit can be obtained to the intensity dependence $I(x)$ under the assumption that a certain fraction of the plume reaches the detector at x without scattering according to the usual Beer's law type behavior for hard-sphere, elastic scattering from fixed targets, i.e., $I(x)=I_0\exp(-ax)$. Here, a is given by the product of the scattering cross section σ and the density of scattering sites, i.e., the Ar density. The mean free path is just $1/a$. A plot of peak intensity as a function of Ar pressure is given in panel (c). From these data a value of 0.36×10^{-15} cm^2 for σ was extracted. The ''atomic cross section,'' defined as π times the Bohr radius squared, is 0.88×10^{-16} cm^2 so the extracted value is quite reasonable; this will be discussed further in Sec. III C.

The results for He are less clear because the peak at 2 μs is not as obvious as in Ar, and the position of the displaced peak depends strongly on pressure. Also, since the He atoms are very light, treating them as fixed scattering centers would not be a good approximation. The contrast between the results for He and Ar is emphasized in panel (d); the model to be described here readily accounts quantitatively for this contrast.

B. Theoretical background

Splitting of the plume flux itself, the origin of which is essential for understanding the plume dynamics, has not been observed in continuum hydrodynamic and gas dynamic calculations. In this short mean-free-path representation, it is the total flux that splits. In the case of a one-fluid representation where plume and background are advected with the same velocity, this is due to the plume plowing the background ahead of it and slowing down in the process.[19,20] In the case of a two-fluid model with a velocity-dependent collisional drag between plume and background[20,21] it is due to the plume reaching the detector first while dragging the background along with it. A scattering model adapted from

Koopman and Goforth[7] does yield splitting but relies on a preionized layer of background gas for Coulombic ion-ion collisions between the plume and background to do so. The validity of these models for the present work is in any case precluded by the fact that the background gas is not ionized and no background gas is observed at the detector using various experimental diagnostics.

Splitting has been equally elusive in direct-simulation Monte Carlo calculations of a Si plume interacting with Ar background gas.[22,23] Although this approach is capable in principle of yielding splitting, as well as many other interesting and important results, the computational demands rapidly become prohibitive for times long enough for a satisfactory description of plume dynamics.

III. DEVELOPMENT OF MULTIPLE-SCATTERING MODEL

We turn now to our multiple-scattering model. Thus far, we have dealt only with a ''quasi-two-dimensional'' (2D) formulation. What is meant by this will become clearer as we proceed. Also, only elastic collisions will be assumed so that the transfer of translational energy into internal excitation energy is, at most, a minor perturbation on the plume dynamics. As stated earlier, the experimental conditions are consistent with this assumption.

A. Elastic scattering

Before proceeding further, it is useful to consider some consequences of elastic collisions.[24] Let v_p and v_b be the velocities of plume and background particles, respectively, before the collision, v_p' and v_b' the corresponding velocities after the collision, and m_p and m_b the masses. Assume first that the collisions are head-on (impact parameter$=0$) and that the velocities are in the positive x direction. Then,

$$v_{px}'=[(m_p-m_b)v_{px}+2m_bv_{bx}]/(m_p+m_b) \tag{1}$$

which yields the well-known result that if $m_p=m_b$, the particles just exchange velocities. Next, consider the cases of Si/He, Si/Ar, and C/Ar where the first element is the plume and the second the background. Carrying out the calculation of v_{px}' for each of these cases, we find, for Si/He,

$$v_{px}'=0.751v_{px}+0.249v_{bx}, \quad v_{px}'>0, \tag{2}$$

for Si/Ar,

$$v_{px}'=-0.174v_{px}+1.175v_{bx} \text{ if } v_{bx}>0.148v_{px}, \text{ then } v_{px}'>0, \text{ otherwise } v_{px}'<0, \tag{3}$$

and for C/Ar,

$$v_{px}'=-0.402v_{px}+0.599v_{bx} \text{ if } v_{bx}>0.671v_{px}, \text{ then } v_{px}'>0, \text{ otherwise } v_{px}'<0. \tag{4}$$

These results show that if the plume particles are heavier than the background particles, as for Si in He, then the plume particles are never scattered in the backward direction. For Si in Ar there will be backscattering until the background particles have attained 15% of the velocity of the plume particles. For light carbon atoms in a heavy Ar background, there will be backscattering until the Ar atoms have been accelerated to 67% of the velocity of the C plume atoms, and this requires many collisions. The inclusion of backscattering in the formalism developed in Sec. III B complicates the implementation and the running time of the computer programs. We found the neglect of backscattering in Si/Ar to make little difference for obtaining the most prominent features of the plume-background interaction, but it is essential in C/Ar which, however, will not be considered further here.

Next, let us consider the more complicated case where the collisions are not head-on but the background particles are stationary. It can be shown (Ref. 24) that when $m_p>m_b$, regardless of the impact parameter, the greatest angle through which m_p is deflected is given by $\sin(m_b/m_p)$. Thus for Si in He, this angle is approximately 8°. If $m_p<m_b$, as in the case of Si/Ar, the velocity of m_p after the collision can have any direction, depending strongly on the value of the impact parameter.

After a head-on collision of a Si atom with a stationary He atom, the latter will have a velocity about 75% greater than that of the Si atom. At first sight, this suggests that when the background gas is He it will simply be swept ahead at a very rapid rate and arrive at the detector well before the plume ions. (If then the He were ionized, the ion probe would detect it before the Si plume.) This would make He very inefficient at slowing down the plume, contrary to what is observed experimentally (see Fig. 1). The way out of this is found by considering the effects of nonhead-on (NHO) collisions on He-He scattering, as explained next.

As we have seen, when the background gas is He, the effect of NHO Si-He collisions on the Si atoms is negligible. The He atoms, on the other hand, can be scattered up to 90° from the x axis with important consequences for the momentum transfer. To take these effects into account in an average way and still maintain an essentially 1D treatment, the total cross section was divided into five concentric rings of equal area, and an average impact parameter for each determined. Given the impact parameter, the scattering angle from the head-on direction (the x direction) and hence the x component of the He atom's momentum for that angle could be calculated. To simplify the calculations, we then averaged the x momentum over the impact parameters. This resulted in reducing the x component of the momentum by more than 30% relative to the head-on approximation.

Let us now consider the effects of He-He collisions themselves. In an exactly head-on collision of a moving He particle with a stationary one, the struck particle moves off with the velocity of the moving particle and the latter is stopped completely so that essentially nothing happens. When NHO collisions are considered, however, it is found that both atoms are moving after the collision, and since the x component of the momentum has to be conserved, and therefore now shared by two atoms, the particle that was initially moving is likely to be drastically slowed. This turns out to be a very efficient mechanism for exchange of momentum between the plume and the background. The reason that the head-on approximation works as well as it does in the calculations described in Sec. IV is because the assumption is made that the Si atoms share their momentum with all of the background mass in a given finite difference cell.

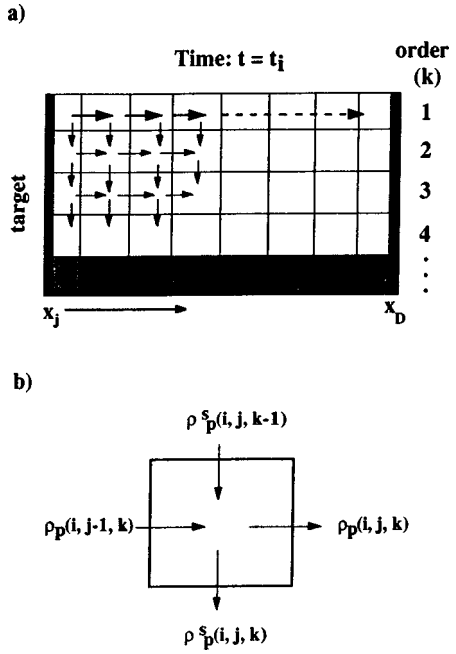

FIG. 2. Schematic illustration of the multiple scattering approach developed here. In panel (a), the k indexes the number of collisions of Si plume atoms with the background atoms. For example, the first order gives the component that gets to the detector without being scattered, the second order component has had one collision, etc. Panel (b) illustrates the conservation of mass in a given cell at a given time. A similar diagram holds for momentum.

As demonstrated in Sec. IV, the assumption of strictly head-on collisions gives good agreement with a large body of the experimental data. Nevertheless, we have tested this assumption by incorporating some of the above effects into what would otherwise be a 1D model, as discussed in Sec. IV. This is one reason why we refer to the model as quasi-2D. That we are able to include approximately some of these effects is due to the fact that the momentum of the ablated plume is predominantly perpendicular to the target surface.

B. Multiple scattering approach

We break the plume up into orders that correspond to the number of collisions that have been made with the background gas. This is shown schematically in Fig. 2(a). As indicated there, the first-order plume is the component that gets to the detector without any scattering, the second-order plume undergoes one scattering event, the third-order plume, two, and so forth. We introduce the following notation: $\rho_p(i,j,k)$ is the density of the kth-order plume in the jth cell at the ith time interval, $\rho_p^s(i,j,k)$ is the density scattered from $\rho_p(i,j,k)$ by collisions, and $\rho_b(i,j,k)$ is the density of background gas. The total density $\rho_p(i,j)$ in the plume can then be written as

$$\rho_p(i,j)=\sum_k \rho_p(i,j,k). \tag{5}$$

A corresponding notation is used for the velocities.

As indicated in Fig. 2(b), at any time and in any spatial cell, collisions may occur that scatter particles from the $k-1$ order into the kth order and from the kth order into the $k+1$ order; of course particles can only be scattered out of the $k=1$ order. While particles can only be transferred to the next higher order by a collision, the density in the individual orders can propagate to give the overall expansion of the plume. The propagation between scattering events is determined by the usual equations for conservation of mass and momentum. We specialize to 1D and write the conservation equations for the plume, including the scattering terms, with $\partial_t \equiv \partial/\partial t$ and $\partial_x \equiv \partial/\partial x$, as

$$\partial_t \rho_p(t,x,k) = -\partial_x[\rho_p(t,x,k)v_p(t,x,k)] + \partial_t \rho_p^s(t,x,k); \tag{6a}$$

$$\begin{aligned}\partial_t \rho_p(t,x,k)v_p(t,x,k) = &-\partial_x[\rho_p(t,x,k)v_p^2(t,x,k) \\ &+ P_p(t,x,k)] \\ &+ \partial_t[\rho_p^s(t,x,k)v_p(t,x,k)],\end{aligned} \tag{6b}$$

with v_p^s, the scattered plume velocity, determined from Eq. (1). The pressure term $P_p(t,x,k)$ was initially neglected but then added in the manner described in Sec. III D. Inclusion of the pressure term and the neglect of inelastic processes effectively eliminates the need to consider the energy conservation equation.

Similar equations can be written for the background but we have generally found it convenient not to resolve the background into its scattered components so as not to complicate the calculations and increase the computational times; we believe the results justify this simplification. The scattering terms, of course, provide the mechanism for the transfer of momentum from the plume to the background since plume scattering from one order to the next higher one is produced only by collisions with the background. That is to say, head-on plume-plume collisions are assumed to be relatively unimportant because they have no net effect on the plume momentum.

We have used the simplest possible discretization scheme to obtain the following finite difference (FD) equations from the differential equations. For the plume,

$$\begin{aligned}\rho_p(i,j,k) = &\rho_p(i-1,j,k) - [\rho_p(i-1,j,k)v_p(i-1,j,k) \\ &- \rho_p(i-1,j-1,k)v_p(i-1,j-1,k)]/v_m \\ &+ \rho_p^s(i,j,k-1) - \rho_p^s(i-1,k),\end{aligned} \tag{7a}$$

$$\begin{aligned}\rho_p v_p(i,j,k) = &\rho_p v_p(i-1,j,k) - [\rho_p v_p^2(i-1,j,k) \\ &- \rho_p v_p^2(i-1,j-1,k)]/v_m \\ &+ \rho_p^s(i,j,k-1)v_p^s(i,j,k-1) \\ &- \rho_p^s(i-1,j,k)v_p^s(i-1,j,k) - [P_p(i-1,j,k) \\ &- P_p(i-1,j-1,k)]/v_m.\end{aligned} \tag{7b}$$

For convenience, the indices on ρ_p have been suppressed in Eq. (7b). For the plume scattering term with plume-background scattering cross section σ_{pb}, we have

$$\begin{aligned}\rho_p^s(i,j,k) = &\rho_p(i,j,k)\rho_b(i-1,j) \\ &\times[v_p(i,j,k) - \overline{v_b}(i-1,j)]\sigma_{pb}\Delta t.\end{aligned} \tag{8}$$

The quantity v_m is the ratio of the Δx and Δt FD cell sizes. The bar over v_b in Eqs. (8) and (9) implies that we have not generally resolved the background into scattering orders, as explained above. In using Eq. (7b) to obtain v_p, it is usually necessary to introduce a lower bound to P_p (and P_b) to ensure that the equation preserves a finite value.

The averaged background is treated in essentially the same manner to give

$$\rho_b(i,j)=\rho_b(i-1,j)-[\rho_b(i-1,j)\overline{v_b}(i-1,j)\rho_b \times(i-1,j-1)\overline{v_b}(i-1,j-1)]/v_m, \tag{9a}$$

$$\rho_b(i,j)\overline{v_b}(i,j)=\rho_b(i-1,j)\overline{v_b}(i-1,j) -[\rho_b(i-1,j)\overline{v_b^2}(i-1,j)-\rho_b(i-1,j-1) \times\overline{v_b^2}(i-1,j-1)]/v_m+B_{pb}-[P_b(i-1,j) -P_b(i-1,j-1)/v_m. \tag{9b}$$

B_{pb} is the transfer of momentum from the plume to the background and is written as

$$B_{pb}=\sum_k \rho_p^s(i,j,k)[v_p(i,j,k)-v_p^s(i,j,k)](m_p/m_b). \tag{10}$$

The use of an average velocity for the background implies that in a collision the entire mass of the background gas in a given finite difference cell will be set in motion. Since this may seem a bit inconsistent with our treatment of the plume, we also carried out some calculations in which the background was resolved into one order that corresponds to some particles in a cell remaining stationary and the velocities of all others being averaged. These calculations, though somewhat more complicated than those for the above equations, are fairly straightforward; the results will be discussed in Sec. IV.

After some experimentation, the FD cell sizes were fixed at $\Delta x=0.05$ cm and $\Delta t=1.25\times10^{-8}$ sec. Real time computations on IBM RISC 6000 machines were less than a minute for the simple model with head-on collisions and no more than a few minutes for the more elaborate NHO versions. This makes the model ideal for real time, on-line optimization and control.

C. Scattering cross section

One might expect the plume-background scattering cross section σ_{pb} to be velocity-dependent, but we have not found it necessary to make it so. In fact, when a velocity dependence was introduced according to more or less standard prescriptions (see Ref. 6, for example) the excellent agreement with experiment obtained with constant cross sections was lost. This may be because there are no ion-ion Coulomb scattering events between plume and background with the experimental conditions used, and the collisions are relatively low in energy compared to those encountered in most plasma processes. Of course, with other experimental conditions, particularly more energetic laser pulses, we might expect the situation to change.

However, this calls attention to another problem. Although a plasma is formed by the laser pulse in the experiments considered here, it is not fully ionized and consists of neutral and singly ionized Si ions, with the neutrals probably the predominant species. As already mentioned, the background gas is always entirely neutral. Therefore, we have to deal with only neutral-neutral, ion-neutral, and Si^+-Si^+ collisions. The last of these can be neglected for the following reasons. First, the expansion of the Si plume is collisionless in the absence of the background gas, and so Si-Si collisions occur only after one of the ions has been scattered by the background gas. Second, the collision of two Si ions will have very little effect on the transport of mass and momentum of the plume itself and will have no direct effect on the transfer of momentum from the plume to the background. Further evidence that Si^+-Si^+ collisions are of little importance under our conditions is given by the fact that the plume expansion in vacuum is described quite well by a single-term half-Maxwellian or Knudsen form, as discussed in Sec. IV B. Consequently, all Si-Si collisions, regardless of the charge states (0 or +1) are of secondary concern.

We conclude that the scattering events of importance here will be primarily those involving collisions between the plume and the entirely neutral background. In this case, the only difference between the scattering cross sections for Si atoms and singly charged ions with the background is a weak polarization contribution that is negligible compared to the dominant nuclear-nuclear repulsion. Therefore, we can write for all plume orders

$$\rho_p(i,j,k)=\rho_p^0(i,j,k)+\rho_p^+(i,j,k), \tag{11}$$

$$\sigma_{pb}^0=\sigma_{pb}^+=\sigma_{pb}, \tag{12}$$

and carry out the calculations as though we were dealing with a neutral plume even though the ion probe detects only the singly charged Si ions. In other words, the kinetics of the propagation and scattering processes are virtually the same for the ions and neutrals. We emphasize once again that these approximations are valid only for the experimental conditions used here and not likely to hold when more energetic, fully ionized plasmas are formed.

There is one important aspect in which the charge state of the Si cannot be ignored, i.e., recombination. The experiments show clearly that light emission due to $Si^+ + e$ recombination occurs throughout the plume expansion. We will not formally include recombination in the calculations of this paper, but preliminary considerations and calculations, based on three-body recombination, as discussed in Ref. 14, suggest that it will further improve the agreement with experiment.

D. Treatment of the pressure term

Calculations without the pressure term in Eqs. (6b), (7b), and (9b) showed that the background gas is very quickly ''snowplowed'' into a peak. This peak traps plume atoms and ions, which themselves form the plume peak that is displaced to long times relative to its vacuum position. However, the background peak is many times greater than that of the plume and this suggests a way of incorporating the pressure term. In the gas dynamical treatment of shock discontinuities in ideal, monatomic gases[25,26] the maximum density in the shock cannot exceed that far in front of the shock by

more than a factor of 4, substantially less than we calculated without the pressure term. While the processes considered in this paper are more complicated than this simple case, we were led to consider further the role of the pressure terms and how to take them into account at least approximately. Since the density of the plume is far less than that of the background at the snowplowed peak, we assumed that the latter controls the physics of the process. More specifically, we assumed that the plume is in thermal equilibrium with the background in this region and that, as in shock-wave theory, the latter is adiabatically compressed during the plume expansion.

The calculation runs as follows. The initial conditions of the background, unlike those for the plume, are known quite well; we denote them by a subscript b and a superscript 0. Then, as the background gas is compressed at any later time, we have for an adiabatic process that

$$P_b/P_b^0=(\rho_b/\rho_b^0)^{\gamma} \quad \text{and} \quad T_b/T_b^0=(\rho_b/\rho_b^0)^{(\gamma-1)/\gamma}, \quad (13)$$

where γ is the ratio of specific heats, c_p/c_v ($=\frac{5}{3}$ for an ideal gas). With T_b known and the assumption of thermodynamic equilibrium, the temperature and pressure of the plume can be determined using the equation of state for an ideal gas.

These results were incorporated into the conservation equations for both the plume and background that were then used for all subsequent calculations. It was found that the peaks in the densities were decreased in height and broadened, as had been anticipated. This resulted in significantly improved agreement with the widths of the experimental plume peaks. Moreover, the temperatures in the shock region were found to be well below that at which appreciable ionization might be expected for either the plume or background. Also, the shock wave properties now fit quite well the results expected from classical shock theory.

IV. CALCULATIONS AND RESULTS

A. Input data and parameters

As already mentioned, the bulk of the experimental data was taken with a pulse energy of nominally 3.0 J/cm^2 and with the detector at 5 cm from the target. It was estimated from past experience and data that approximately 5×10^{15} atoms and singly charged ions were ejected per pulse. Although the ratio of charged ions to neutral atoms in the plume is not known, it is not likely to be a major concern for most of the calculations of plume dynamics for reasons already discussed. However, recombination does occur as the plume species move from the target to the detector, and this may explain some of the discrepancies that are observed between experiment and theory.[14] From the vacuum results, it can be determined that the maximum velocity of the plume particles is $\sim4\times10^6$ cm/sec, with the peak of the ion probe signal corresponding to approximately 2.5×10^6 cm/sec.

B. Starting pulse and vacuum results

The propagation of the plume in the absence of a background gas was investigated extensively. Equations (7a) and (7b) for conservation of mass and momentum in the plume but without the scattering terms, i.e., with $\sigma_{pb}=0$, were used together with various assumptions for ρ^0, the starting pulse at $t=t_0$. Kelly and Dreyfus[27] have discussed at length the so-called half-range Maxwellian and Knudsen forms given, respectively, by

$$\rho_M^0(v_x,v_y,v_z)=N_M\exp[-m(v_x^2+v_y^2+v_z^2)/2kT_s] \quad (14)$$

and

$$\rho_K^0(v_x,v_y,v_z)=N_K\exp\{-m[(v_x-u_K)^2+v_y^2+v_z^2]/2kT_K\}. \quad (15)$$

T_S is the ''surface temperature'' of the Si target and T_K is related to it in the manner discussed in Ref. 27. T_S is of the order of 35 eV ($\sim4\times10^5$ K) and T_K somewhat less for the laser pulses used in the experiments. These temperatures are far above the vaporization temperature of Si and come about because of formation of the plasma (although the details of the breakdown mechanisms are still not entirely clear). The preexponential factors N_M and N_K contain normalization factors and a factor giving the number of atoms ablated with each pulse.

It was found that the second of these two forms generally gave the better results. However, a linear combination of two terms of the form of Eq. (15) gave a somewhat improved fit, and it appears that the vacuum plume may be made up of two components. Further study of this is needed, but we found that small variations in the form of the starting vacuum pulse made little difference to the calculations for plume expansion in the presence of a background gas, except for some of the lower background pressures. All of the results given in this paper were obtained with the Knudsen form.

In order to convert the densities given by Eqs. (7a) and (9a) into the fluxes that are observed with an ion probe detector, it is necessary to multiply by the velocity squared and divide by the third power of the time, as discussed in Ref. 27. Here we remark that a t^{-2} factor accounts for the fact that any small velocity components in the y and z directions will cause the plume particles to miss the detector, depending on the target-detector distance and the acceptance dimensions of the detector. This is another reason why it is appropriate to refer to the model as quasi-2D.

C. Plume expansion in a background gas

Figure 3 gives an overall comparison of the calculated and experimental plume results for Si/Ar and Si/He obtained from the simplest version of the general model developed here. This is one in which only head-on collisions are considered and the background gas is assigned an average velocity, as discussed in Sec. III B. The pressure term was included according to the development in Sec. III D. Only the scattering cross section was allowed to vary freely in going from Ar to He while the N_K in Eq. (15) was taken approximately 10% less for He than for Ar in order to be consistent with the experimental conditions. For Ar, the cross section and N_K were fixed by obtaining a reasonably good fit to the data at 80 mTorr, after which only the Ar pressure was assigned the values at which the data were taken. The same procedure was followed for He by fitting the 200 mTorr data.

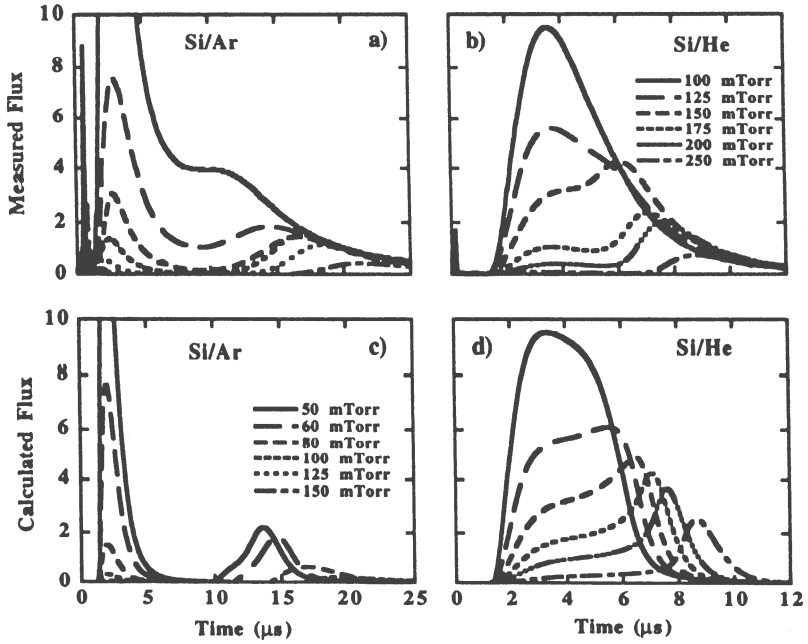

FIG. 3. Overall comparison of calculated and experimental results for the two background gases. This agreement is obtained by changing only the value of σ_{pb} in going from He to Ar and slightly altering the starting laser pulse to be consistent with the conditions under which the experimental data were obtained.

N_K is $\sim 10^{15}$ cm^{-3} in both gases and $\sigma_{pb}=5.1\times10^{-16}$ cm^2 in Ar and 3.0×10^{-16} cm^2 in He, which can be compared to the ''atomic cross section'' ($=\pi a_0^2$ with a_0 the Bohr radius) of 0.88×10^{-16} cm^2. Also, the ratio $\sigma_{pb}(\mathrm{Si/Ar})/\sigma_{pb}(\mathrm{Si/He})=1.69$ is very close to $[r(\mathrm{Si})+r(\mathrm{Ar})]^2/[r(\mathrm{Si})+r(\mathrm{He})]^2=1.66$ where $r(\mathrm{Si})=1.17$ Å is the covalent radius of Si and $r(\mathrm{Ar})=1.91$ Å and $r(\mathrm{He})=1.22$ Å are van der Waals radii.

It is apparent that the calculated results give excellent general agreement with a large quantity of experimental data. The ''plume splitting'' is apparent in both background gases. However, there are two noticeable discrepancies. In He, a minimum between the first (in time) shallow peak and the delayed sharp peak is not resolved in the calculations. We believe this may be due to the neglect of recombination.[14] In Ar, the intensity drops nearly to zero between the two peaks in the calculated curves whereas it does not in the experimental results. This is most likely due to the assumption of only head-on collisions, a conclusion we will partially substantiate shortly. A more detailed comparison of the calculated and measured ion-probe signals from Fig. 3 for Si in He is given in Ref. 14.

The resolution of the total scattered intensity into its component parts is shown in Fig. 4 for the cases of 80 mTorr of Ar and 175 mTorr of He. Only the first (no collisions) and subsequent even orders are shown for He. To obtain convergence, it is necessary to include many more scattering orders for Si/He than for Si/Ar. For the same background pressure, each collision in He transfers only a small amount of momentum to the background compared to the Ar case. Thus, in order to get the same magnitude of splitting experimentally it is necessary to go to higher pressures for the former. In this connection, it should also be noted that the second-order plume in Si/He is barely split off from the unscattered first-order plume, whereas in Si/Ar the first-order plume is already well resolved. This is a direct result of the much greater slowing down of the Si ions by the massive Ar atoms compared to the light He atoms. In fact, had the transfer of momentum to the background not been averaged over the scattering orders, it would have been found that at least a few He atoms actually get to the detector before the Si ions, as was verified by a separate calculation. That no such fast He

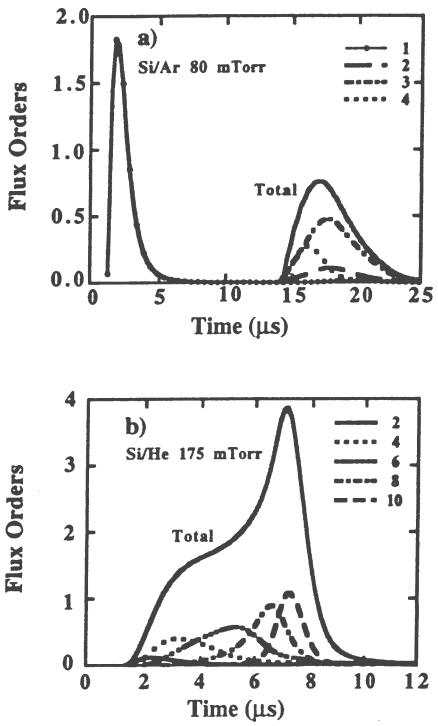

FIG. 4. Resolution of the plume into scattering orders in the two background gases for the two pressures indicated. The number of orders required for convergence is large in He so that only the first (unscattered) and subsequent even ones are shown.

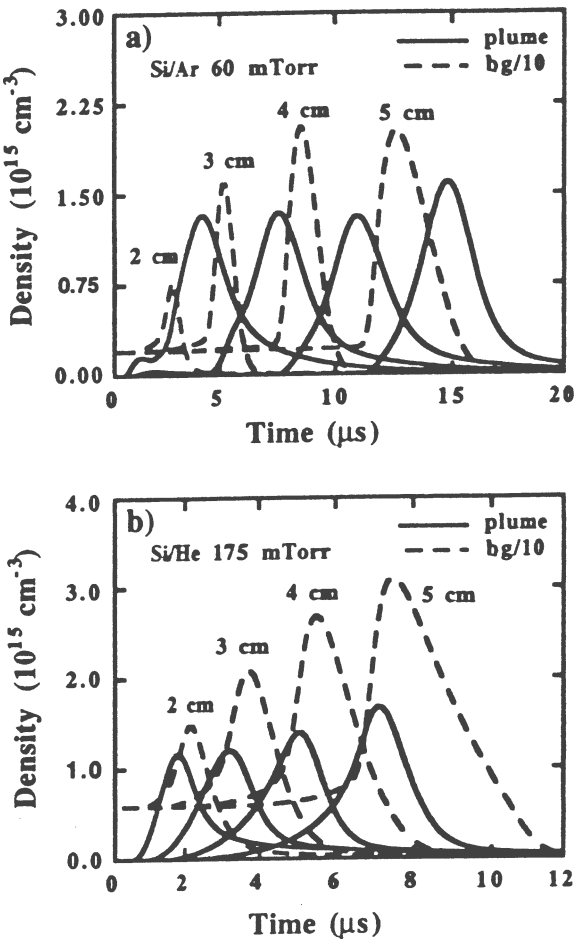

FIG. 5. Comparison of the densities of the plume and the background in the regions of the slow peaks for several different distances of the detector from the target for the indicated background pressures. This figure shows clearly how the two peaks build up with distance from the detector and how the plume peak is trapped behind or within the background peak.

ions were detected experimentally is another indication that the background gas is not ionized under the conditions used here.

D. Dynamics of the background gas

In Fig. 5, the densities of the Si plume and the background gases as functions of time and distance from the target are shown for two typical cases. Note that the background density as shown is roughly an order of magnitude greater than the plume density.

It can be seen, as previous calculations have indicated,[19,20] that the background gas density appears to be ''snowplowed'' into a sharp peak by the momentum transferred from the plume, while the plume itself also piles up because it is unable to completely penetrate the background peak. However, considerable interpenetration of the two peaks does occur so that ''snowplowing'' is not an entirely accurate description. In fact, the background gases behave somewhat differently in this regard. In Si/Ar, the maximum of the Ar distribution slightly precedes that of the Si peak for all distances from the target, while in Si/He the converse is true. Whether or not there is a fundamental reason for this is not clear at present.

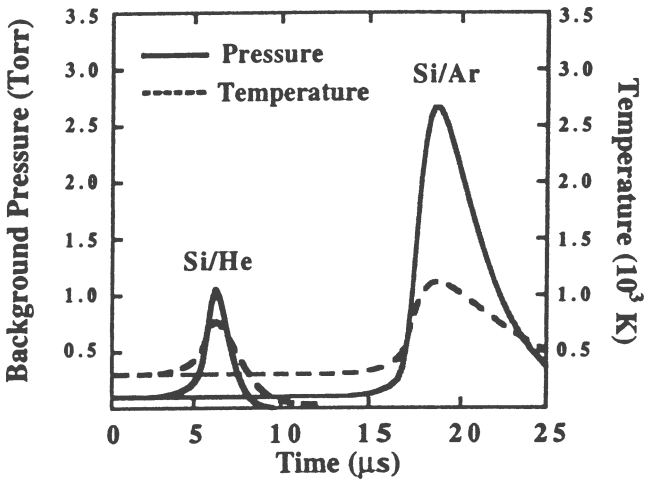

FIG. 6. Calculated background pressure and temperature profiles using the approach described in Sec. III D.

The plume results for 2 cm in the Si/Ar case show a small bump near 2 μs. In fact, each of the plume curves has such a bump but it is generally unresolved on the scale of the figure. When we convert from densities to fluxes these bumps grow into the unscattered peaks ($k=1$) of Figs. 4(a) and 4(b). This emphasizes the importance of the time factors discussed above and in Ref. 27. Recall that the distributions of Eqs. (14) and (15) have to be divided by the fifth power of time to obtain the vacuum flux. In the density calculations of this section, one factor of $1/t$ is included automatically through the propagation equations so that to obtain the flux we must divide through by t^4.

From results such as those in Fig. 5, the velocities of both the plume and background peaks as functions of time and initial background pressure can be calculated. For example, in 60 mTorr of Ar, the velocity of the plume peak at 5 cm has been slowed by nearly an order of magnitude compared to its vacuum velocity of 2.5×10^6 cm/sec and the plume and background peaks are moving at very nearly the same velocities. The situation in 175 mTorr of He is similar in that the peaks of the plume and background at 5 cm (and other distances) have nearly the same velocities, but the plume velocity is only a factor of 5 less than its value in vacuum. In all of these calculations the total densities and momenta are very well conserved.

In Fig. 6, typical results for the temperature and pressure in the background are shown. We believe that the results in Fig. 5 that show the background density to be approximately an order of magnitude greater than that of the plume in the region of interest substantiates the approximations we used for calculating these quantities. The plume and background temperatures are the same since thermodynamic equilibrium between the two was assumed. It will not be shown here, but the inclusion of the pressure term in the propagation equations reduced the height of the background peak by a factor of about 4 and broadened it accordingly. The peak position was not changed significantly. The temperature rise due to the compression of the background gas is relatively modest compared to that required for ionization of any of the three gases involved, so that our initial assumptions about their ionization states seem well justified, although recombination of Si^+ and electrons is expected to be important.[14]

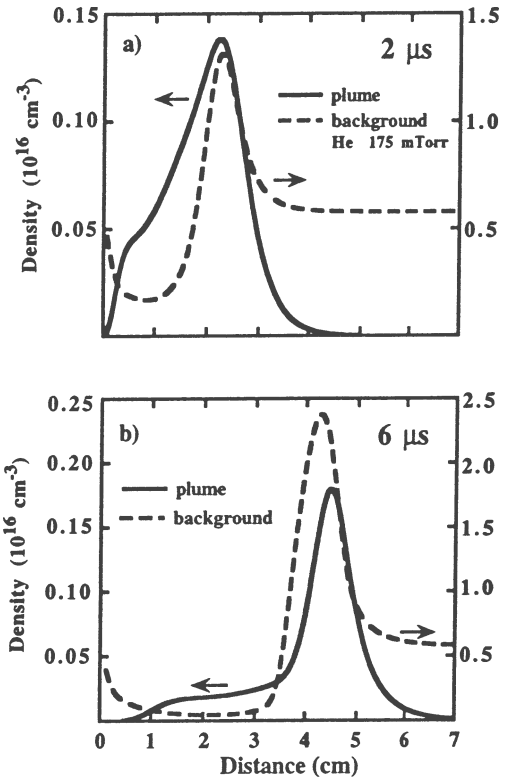

FIG. 7. Shock front behavior for Si in 175 mTorr of He at two different times. Note that the background density is approximately an order of magnitude greater than the plume density.

We saw in Sec. III D that for an ideal gas the maximum density in the shock wave cannot exceed the density far in front of the maximum by more than a factor of 4. The results shown in Fig. 7 for Si in 175 mTorr of He at two different times illustrate that this is indeed the case for our calculations. In none of the calculations we have checked has this maximum ratio of four been exceeded, within the accuracy of the calculations. Because the density of the plume is approximately an order of magnitude less than that of the background, this remains approximately true even for the combined densities. It should be noted that the dashed curves show clearly how the background density is swept out of the region closest to the target and piled up to form the shock front. At the same time, the plume is compressed into the same region because the Si atoms are unable to penetrate the much denser background peak.

E. Effects of nonhead-on collisions

All of the results given above were obtained under the assumption that all collisions were head-on. Since the probability of truly head-on collisions is virtually zero, considerable effort was put into extending the modeling beyond this approximation. Some of the results are discussed here.

In Sec. III A it was shown that Si atoms that collide with stationary He atoms will be deflected through angles no greater than 8°, regardless of the impact parameter, so that the head-on approximation is quite good for the Si ions. For the He atoms it is not. To account for this, we split the He atoms into two groups, corresponding to those in a given cell that at any time are still stationary because they have not yet been hit by a Si atom and all others which have been hit. This latter group is assigned an average velocity. In the previous calculations, even the He atoms that had not been hit were included in the averaging process. Now however, there is a group of moving He atoms and a group that is still stationary. The former may collide with the latter but this would have no effect if the collisions were head-on since the two would just exchange velocities. We took into account the NHO collisions in the manner already described in Sec. III A. Stationary He atoms can then be set in motion by being hit by both Si atoms and moving He atoms.

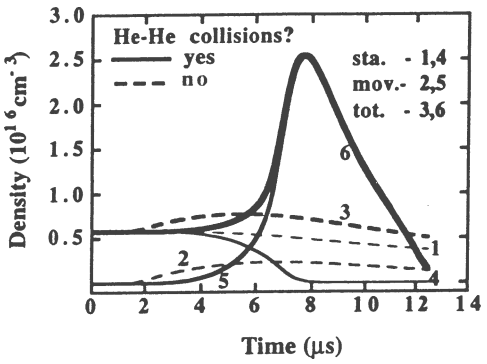

FIG. 8. Illustration of the role of NHO collisions for the case of Si in 175 mTorr of He. See text for discussion of this rather complex figure.

The importance of the NHO collisions is illustrated in Fig. 8 where the time dependence at 5 cm of the He background density at 175 mTorr is shown. Curves 1, 2, and 3, shown dashed, are for the case in which the He-He collisions are neglected. Curve 1 gives the stationary component, curve 2 the moving component, and curve 3, the total density. Curves 4, 5, and 6 give the corresponding results when He-He collisions are included. It is apparent that without this term a large fraction of the He atoms remain stationary and those that are hit simply run away from the rest. With the term, almost all of the background is set in motion and the velocities are such that the snowplowed peak becomes the most prominent feature. If curve 6 is compared to the He background on Fig. 5(b), it can be seen that they resemble each other closely. In other words, by averaging the momentum over all the background mass in a given cell in the head-on approximation, we arrive at essentially the same result as for the more realistic NHO calculations. Of course, changes in N_K and σ_{pb} must be introduced, but these are not particularly large.

Nevertheless, the calculations do show that a few He atoms can reach the detector before the plume particles and they would show up as an ion probe signal if they were charged. On the whole, however, the results are so similar to those already given for the simple head-on model, and with only minor changes in the parameters, that we will not give figures for them here.

Turning now to Ar, we concluded that the failure of the simple model to fill in the region between the fast and slow peaks in Fig. 3 for some of the lower Ar pressures was due to neglect of those collisions at large impact parameters for which the scattering angle is small. (For strictly head-on collisions with stationary Ar atoms the Si atoms will always be backscattered by 180°. It is only after the background has

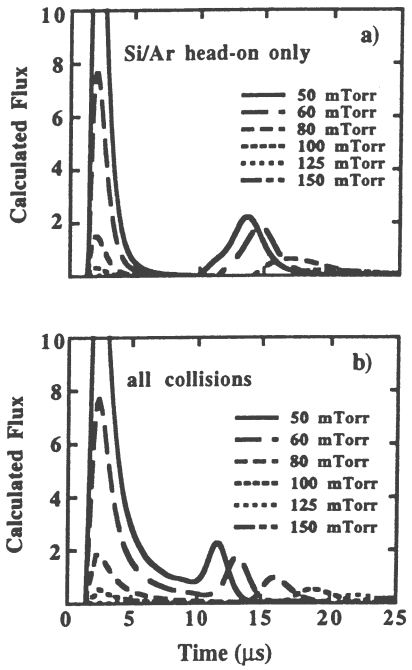

FIG. 9. Results of calculations for Si/Ar using an extension of the basic model in which NHO collisions are partially taken into account, as described in the text. These results show how the region between the two peaks begins to fill in as collision processes with a range of impact parameters are taken into account.

been set in motion that forward scattering begins to occur, as described in Sec. III A.) To try to verify this, we modified the model to allow for five different impact parameters as described above for the He calculations. The results are shown in Fig. 9 where it can be seen that the region under discussion does indeed begin to fill in, as anticipated. This particular aspect of the modeling is not crucial for understanding the plume-splitting problem and other important aspects of plume and background propagation and so it has not been pursued further at this time.

V. SUMMARY AND CONCLUDING DISCUSSION

We have developed a relatively simple model of the expansion of a laser-ablated Si plume into He and Ar background gases that gives good agreement with most of the experimental results. Momentum is transferred from the plume to the background by multiple scattering of the plume atoms from those of the background gas. Propagation of the plume and background is achieved by introducing the conservation equations of gas dynamics. The previously unexplained phenomenon of plume splitting is seen to occur in Ar because there is a finite probability that some of the Si target atoms will reach the detector without any collisions with the heavy background gas atoms, giving rise to the fast peak. Even single collisions are enough to significantly retard plume atoms and the cumulative effect of all scattered components produces the second peak. In He, the process is more complicated because one or two collisions do not split the scattered component very far from the vacuum peak and several orders may partially overlap in this region. The complex interplay of the various scattering orders then determines whether or not two peaks will be resolved, with recombination possibly playing an important role in this connection.

Part of the success of the modeling may be due to the choice of an experimental system for which the various approximations clearly apply. Therefore, questions about the general applicability of our approach may arise. While it is apparent that modifications may have to be made for specific cases, we believe that the ubiquitous nature of plume splitting shows that the model captures the essential physics of the phenomenon. For example, we have constructed a version of the model to deal with graphite ablated into a background gas of Ar. As pointed out in the subsection on elastic scattering, the large mass difference between C and Ar means that the backscattering of the C is an important effect. While we are able to incorporate this into the model, it greatly complicates the equations and the programming because reflection of the backscattered C atoms from the target may be an important effect. This requires further study.

With the above in mind it is worth emphasizing that, in choosing an experimental system with which to work, the interaction between experiment and theory will be facilitated if the background gas is lighter than the plume gas because the effects of backscattering will then be minimized.

ACKNOWLEDGMENTS

We would like to thank C.-L. Liu for extended discussions during the earliest stages of this work and T. Makimura for valuable comments on the final manuscript. This work was supported in part by Laboratory Directed Research and Development Funds and by the Division of Materials Sciences, U.S. Department of Energy, under Contract No. DE-AC05-96OR22464, with Lockheed Martin Energy Research Corporation. K.R.C. was supported by the National Science Council of the Republic of China.

*Permanent address: Department of Physics, National Cheng Kung University, Tainan, Taiwan 701, Republic of China.

[1] H. M. Smith and A. F. Turner, Appl. Opt. **4**, 147 (1965). These authors appear to have been the first to demonstrate thin-film deposition by laser ablation.

[2] For recent reviews of many current aspects of thin-film formation by pulsed-laser deposition see the various chapters in the volume *Pulsed Laser Deposition of Thin Films*, edited by D. B. Chrisey and G. K. Hubler (Wiley, New York, 1994).

[3] D. Dijkkamp, T. Venkatesan, X. D. Wu, S. A. Shaheen, N. Jisrawi, Y. H. Min-Lee, W. L. McLean, and M. Croft, Appl. Phys. Lett. **51**, 619 (1987); X. D. Wu, D. Dijkkamp, S. B. Oagale, A. Inam, E. W. Chase, P. F. Micelli, C. C. Chang, J. M. Tarascon, and T. Venkatesan, *ibid.* **51**, 861 (1987).

[4] J.-M. Triscone, O. Fischer, O. Brunner, L. Antognazza, A. D. Kent, and M. G. Karkut, Phys. Rev. Lett. **64**, 804 (1990); Q. Li, X. Xi, X. D. Wu, A. Inam, S. Vadlamannati, and W. L. McLean, *ibid.* **64**, 3086 (1990); D. H. Lowndes, D. P. Norton, and J. D. Budai, *ibid.* **65**, 1160 (1990).

[5] For an extended discussion of the early work, see the well-known book by J. F. Ready, *Effects of High-Power Laser Radiation* (Academic, New York, 1971).

[6] D. W. Koopman, Phys. Fluids **15**, 1959 (1972).
[7] D. W. Koopman, and R. R. Goforth, Phys. Fluids **17**, 1560 (1974).
[8] For a recent review, see D. H. Lowndes, D. B. Geohegan, A. A. Puretsky, D. P. Norton, and C. M. Rouleau, Science **273**, 898 (1996).
[9] D. B. Geohegan and A. A. Puretzky, Appl. Surf. Sci. **96-98**, 131 (1996).
[10] D. B. Geohegan and A. A. Puretzky, Proc. SPIE **2405**, 15 (1995).
[11] C. M. Rouleau, D. H. Lowndes, J. W. McCamy, J. D. Budai, D. B. Poker, D. B. Geohegan, A. A. Puretzky, and S. Zhu, Appl. Phys. Lett. **67**, 2445 (1995).
[12] E. Werwa, A. A. Seraphin, L. A. Chiu, C. Zhou, and K. D. Kolenbrander, Appl. Phys. Lett. **64**, 1821 (1994).
[13] I. A. Movtchan, W. Marine, R. W. Dreyfus, H. C. Lee, M. Sentis, and M. Autric, Appl. Surf. Sci. **96–98**, 251 (1996); T. Yoshida, S. Takeyama, Y. Yamada, and K. Mutch, Appl. Phys. Lett. **68**, 1772 (1996).
[14] R. F. Wood, K. R. Chen, J. N. Leboeuf, A. A. Puretsky, and D. B. Geohegan, Phys. Rev. Lett. **79**, 1571 (1997).
[15] R. F. Wood, J. N. Leboeuf, K. R. Chen, D. B. Geohegan, and A. A. Puretsky, *Proceedings of 1997 Conference on Laser Ablation* [Appl. Surf. Sci. **127-129**, 151 (1998)].
[16] R. F. Wood and G. A. Geist, Phys. Rev. Lett. **57**, 873 (1986); Phys. Rev. B **34**, 2606 (1986).
[17] D. B. Geohegan, Thin Solid Films **220**, 138 (1992).
[18] A review of many of these is given by D. B. Geohegan, in *Pulsed Laser Deposition of Thin Films* (Ref. 2), Chap. 5.
[19] A. Vertes, in *Laser Ablation: Mechanisms and Applications*, edited by J. C. Miller and D. B. Geohegan, AIP Conf. Proc. No. 288 (AIP, New York, 1994), p. 275.
[20] J. N. Leboeuf, K. R. Chen, J. M. Donato, D. B. Geohegan, C. L. Liu, A. A. Puretzky, and R. F. Wood, Phys. Plasmas **3**, 2203 (1996).
[21] P. W. Rambo and J. Denavit, J. Comput. Phys. **98**, 317 (1992).
[22] J. C. S. Kools, J. Appl. Phys. **74**, 6401 (1993).
[23] D. L. Capewell and D. G. Goodwin, Proc. SPIE **2403**, 49 (1995).
[24] We have found particularly useful the exposition in L. D. Landau and E. M. Lifshitz, *Mechanics* (Pergamon, Oxford, 1960).
[25] M. N. Kogan, *Rarefied Gas Dynamics* (Plenum, New York, 1969).
[26] Y. B. Zel'dovich and Y. P. Raizer, *The Physics of Shock Waves and High-Temperature Hydrodynamic Phenomena* (Academic, New York, 1966).
[27] R. Kelly and R. W. Dreyfus, Surf. Sci. **198**, 263 (1988).